Journal of Applied Fluid Mechanics, Vol. 9, No. 4, pp. 1559-1568, 2016.
Available online at www.jafmonline.net, ISSN 1735-3572, EISSN 1735-3645.
DOI: 10.18869/acadpub.jafm.68.235.24668

An Approximate Method for the Evaluation of the Normal Force Acting on a Flexible Plate Normal to the Wind Flow

J. F. Hu[1†] and W. X. Wang[2]

[1] *Department of Aeronautics and Astronautics, Engineering School, Kyushu University, Fukuoka City, Fukuoka, 819-0395, Japan*
[2] *Research Institute for Applied Mechanics, Kyushu University, Kasuga, Fukuoka, 816-8580, Japan*

†*Corresponding Author Email: hu-junfeng@riam.kyushu-u.ac.jp*

(Received February 2, 2015; accepted September 15, 2015)

ABSTRACT

The purpose of this paper is to develop an approximate method for the evaluation of the normal force acting on a flexible plate normal to the wind flow and the deformation of the plate. A theoretical modelling is firstly proposed to predict the relationship between the normal drag coefficient of a rigid curved-plate and the configuration of the plate with the aid of a series of numerical analyses of structure and fluid dynamics. Then, based on the theoretical modelling, an approximate method for the evaluation of the normal force acting on the plate and the deformation of the plate is constructed using only the iteration of structure mechanics analysis, instead of conventional complex iterations of fluid-structure coupling analysis. Simulation tests for 3D flexible plates with different lengths and different material moduli are conducted. Also a comparative simulation test of a 3D flexible plate used in a previous experiment is performed to further confirm the validity and accuracy of the approximate method. Numerical results obtained from the approximate method agree well with those obtained from the fluid dynamics analysis as well as the results of the previous wind tunnel experiment.

Keywords: Wind flow; Flexible plate; Fluid-structure interaction; Normal force; Approximate method.

NOMENCLATURE

A	area of the plate
C_D	drag coefficient of a rigid flat-plate normal to the flow
C_{D_theory}	drag coefficient of a rigid curved-plate based on theoretical modelling
C_{N-CFD}	normal force coefficient of a rigid curved- plate obtained from CFD simulation
C_{N-real}	real normal force coefficient of a flexible plate normal to the flow
C_{N_theory}	normal force coefficient of a rigid curved-plate based on theoretical modelling
ds	an arbitrary infinitesimal element of rigid curved-plate
E	Young's modulus
F_N	total normal force acting on an the plate
$F_{N-theory}$	total normal force acting on a rigid curved-plate obtained from theoretical modelling
$f(\tilde{\ })$	correction function
L	length of the plate
p	average pressure acting on the plate
p_{-real}	real averaged pressure acting on a flexible plate
$p_{-theory}$	average pressure acting on a rigid curved-plate obtained from theoretical modelling
s	arbitrary location on the curved plate
T	thickness of the plate
u_x	x component of displacement
u_y	y component of displacement
W	width of the plate
V	wind velocity
V_N	velocity component normal to the curved surface
V_T	velocity component along the tangential direction of the curved surface
	correction coefficient
–	chord angle of the arbitrary infinitesimal element along the curved plate
–~	chord angle of the curved plate
–~ –real	real chord angle of a flexible plate normal to the flow
3	Poisson's ratio
°	density of air

1. INTRODUCTION

A flexible plate normal to the wind flow is a typical and classic problem of fluid-structure interaction (FSI), of direct relevance to many natural phenomena. For instance, leaves of plant, flexible fiber, and plates roll up in a high wind to reduce the drag and avoid damage as reported by Vogel (1989. 2009), Alben *et al*. (2002, 2004), Schouveiler and Boudaoud (2006), and Gosselin *et al*. (2010). Furthermore, this problem is also of relevance to many practical applications such as commercial plates and turbine blades (Maheri *et al*. (2007); Liu 2009; Hoogedoorn *et al*. (2010)). Many research efforts (e.g., Fage and Johansen (1927), Kiya and Arie (1977), Chein and Chung (1988), Kinsely (1990), Okajima (1990), Letchford (2001), Shimada and Ishihara (2002), and Breuer *et al*. (2003)) have been contributed to the investigation of the dynamic behaviors of the flow around a rigid-plate, such as drag coefficient, lift coefficient, Strouhal numbers, velocity fluctuation behind the plate, and vortex behaviors. Relatively few studies (Vogel (1989, 2009), Alben *et al*. (2002, 2004), Schouveiler and Boudaoud (2006), and Gosselin *et al*. (2010), Campbell and Paterson, (2011); Lee and Lee, (2012)) have been focused on the evaluation of the wind pressure acting on a flexible plate and the deformation of the plate. On the other hand, the wind pressure acting on a deformable plate and the deformation of the plate are important parameters in the strength design of the plate and its supportive structure in practical applications.

In general, it is extremely difficult to derive an analytical solution for the evaluation of the wind pressure acting on a flexible plate because of the strong nonlinearity in the coupling of the fluid flow and the plate deformation. Rigorous evaluation requires complex fluid-structure coupling analysis although many numerical methods have been developed as reviewed by Hou *et al*. (2012) and Degroote (2013), such as the arbitrary Lagrangian-Eulerian (ALE) finite element method (Kim *et al*. (2007), Peskin (2002)) and the Boltzman-Lattice method (Feng and Michaelides (2004), Lee *et al*. (2012)). Complex iteration procedures of numerical calculations related to the alternative fluid and structure analyses are cumbersome and error-prone in the rigorous FSI numerical analysis. Therefore, developing a relatively simple numerical method to evaluate the wind pressure acting on a deformable plate is quite useful in various practical applications.

In this paper, we are interested to develop an approximate numerical method for the evaluation of the normal force acting on a flexible plate normal to the wind flow and the deformation of the plate. The averaged pressure is defined by the normal force divided by the plate area. A theoretical modelling is proposed to approximately describe the relationship between the normal drag coefficient of a rigid curved-plate in the flow and its configuration with the aid of a series of regular numerical calculations of fluid dynamics and structure mechanics. Based on the theoretical curve of the normal drag coefficient and the configuration of the rigid curved-plate, an approximate method for the evaluation of the normal force acting on the plate and the deformation of the plate is constructed using only the iteration of structure mechanics analysis, instead of conventional complex iterations of fluid-structure coupling analysis. Simulation tests for 3D flexible plates with different lengths and different material moduli are conducted. Also a comparative simulation test of a 3D flexible plate used in a previous experiment is performed to further confirm the validity and accuracy of the approximate method.

2. APPROXIMATE METHOD

In this section, a theoretical formulation to describe the relationship between the normal drag coefficient of a rigid curved-plate and the configuration of the plate is first derived. Then, based on the theoretical formulation, an approximate numerical method is constructed to evaluate the normal force acting on a flexible plate and the deformation of the plate using only the iteration of structure mechanics analysis, instead of the conventional complex fluid-structure coupling analysis.

2.1 Theoretical Modelling

A flexible plate with upper end fixed normal to the wind flow is considered, as shown in Fig. 1(a). The length, width, and thickness are denoted by *L*, *W*, and *T*, respectively. The plate subjected to wind pressure tends

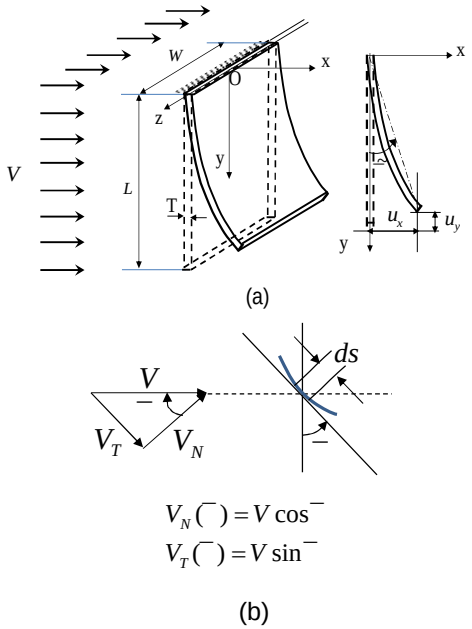

Fig. 1. The schematic of a flexible plate normal to wind flow.

to bend towards the flow direction to reduce drag. Dashed line denotes the plate before deformation. The displacements of free end are denoted by u_x and u_y. The deformed configuration is described by the chord angle $\tilde{\alpha}$ between the vertical line and the line connecting the fixed end and the free end of the plate. In general, this is a complex fluid-structure coupling problem, the pressure acting on the plate is complicatedly distributed on the plate surfaces and fluctuates around its mean value over time (Fage and Johansen (1927), Chein and Chung (1988), and Lee and Lee (2012)). In present study, as the first approximation, it is assumed that the deformed plate in uniform and steady wind flow is under a quasi-static state and that the mean pressure is uniformly distributed on the plate surface. Therefore, the deformed plate under the quasi-static state in the wind flow can be considered as an equivalent rigid curved-plate. Furthermore, the effect of the viscous drag along the tangential direction of the plate surface due to the fluid viscosity on the deformation of the plate is considered to be very slight compared to the wind pressure normal to the surface so that only the normal force is considered in the present study. In addition, for the sake of simplicity, the effect of gravity on the deformation of plate is not considered hereafter.

Based on the above assumptions, consider the wind flow acting on an arbitrary infinitesimal element *ds* of a rigid curved-plate, as shown in Fig. 1(b). *V* is the wind velocity, V_N and V_T are the velocity components normal to the curved surface and along the tangential direction of the curved surface, and *s* is the Lagrangian coordinate defined along the mid-plane of the plate from its fixed end to its free end, respectively. Therefore, the total normal force produced by the wind flow with velocity *V* on the curved plate can be expressed by

$$F_{N-theory} = \frac{1}{2}\int_0^L \rho \cdot (V \times \cos\beta)^2 W C_D ds \tag{1}$$

Where ρ $(=1.225\ kg/m^3)$ is the density of air, β is the tangential angle of the curved plate at location s, and C_D is the drag coefficient of an equivalent rigid flat-plate ($L \times W \times T$) normal to the flow. C_D can be find from books of fluid mechanics (e.g. White 1998) for regular 3D plates or can be obtained from fluid dynamic analysis using a computational fluid dynamics (CFD) codes. Generally, $\beta(=\beta(F_{N-theory}, s))$ is a function of the normal force and the location *s* along the curved plate, and this equation is actually an integral equation of fluid-structure coupling. It is difficult to obtain the exact solution. In order to express the total normal force $F_{N-theory}$ in an explicit formulation, we assume that the total normal force $F_{N-theory}$ can be approximately expressed by

$$F_{N-theory}(\tilde{\alpha}) = \frac{1}{2}\rho \cdot V^2 A C_D f(\tilde{\alpha}) \cos^2\tilde{\alpha}, \tag{2-a}$$

$$A = L \times W \tag{2-b}$$

Where A denotes the area of the plate, $\tilde{\alpha}$ denotes the chord angle of the curved plate (Fig. 1(a)) and is used to characterize the configuration of the curved plate, and $f(\tilde{\alpha})$ is a correction function which is used to correct the errors caused by the above simplification because Eq. (2-a) is not a rigorous solution of the integral equation of Eq. (1). Then the average pressure $p_{-theory}$ acting on the curved plate can be calculated by

$$p_{\_theory} = \frac{F_N(\tilde{\alpha})}{A} = \frac{1}{2}\rho \cdot V^2 C_D f(\tilde{\alpha}) \cos^2\tilde{\alpha} \tag{3}$$

From Eq. (3), the normal drag coefficient of the curved plate can be expressed by

$$\begin{aligned} C_{N-theory}(\tilde{\alpha}) &= \frac{p_{\_theory}(\tilde{\alpha})}{0.5 \cdot \rho \cdot V^2} = \frac{F_N(\tilde{\alpha})}{0.5 \cdot \rho \cdot V^2 A} \\ &= C_D f(\tilde{\alpha}) \cos^2\tilde{\alpha} \end{aligned} \tag{4}$$

And the conventional drag coefficient is expressed by

$$\begin{aligned} C_{d-theory}(\tilde{\alpha}) &= \frac{F_d(\tilde{\alpha})}{0.5 \cdot \rho \cdot V^2 A} \\ &= \frac{F_N(\tilde{\alpha}) \times \cos\tilde{\alpha}}{0.5 \cdot \rho \cdot V^2 A} \\ &= C_{N-theory}(\tilde{\alpha}) \times \cos\tilde{\alpha} \\ &= C_D f(\tilde{\alpha}) \cos^3\tilde{\alpha} \end{aligned} \tag{5}$$

Observing Eq. (4) and Fig. 1(a), it is recognized that $\tilde{\alpha} = 0$ and $\tilde{\alpha} = \pi/2$ correspond to the two special cases of a rigid flat-plate normal and parallel to the wind flow, respectively. Therefore, according to fluid mechanics, the normal drag coefficient $C_{N-theory}(\tilde{\alpha})$ should satisfy $C_{N-theory}(0) = C_D$ and $C_{N-theory}(\pi/2) = 0$. The correction function $f(\tilde{\alpha})$ should satisfy $f(0) = 1$ and $f(\pi/2) < \infty$. As a result, $f(\tilde{\alpha})$ is assumed here by

$$f(\tilde{\alpha}) = 1 + \quad \sin^2\tilde{\alpha} \tag{6}$$

Where parameter is a constant which is determined from the comparison between the curve $C_{N-theory}(\tilde{\alpha})$ obtained from Eq. (4) and the curve $C_{N-Exp.}(\tilde{\alpha})$ obtained from experiment or $C_{N-CFD.}(\tilde{\alpha})$ obtained from a series of CFD calculations of rigid curved-plates with chord angles $\tilde{\alpha}_i (0 < \tilde{\alpha}_i < \pi/2; i = 1, 2, \cdots, k)$. In the present study, CFD calculations are employed to determine the curve $C_{N-CFD.}(\tilde{\alpha})$. The geometries of rigid curved-plates with chord angles $\tilde{\alpha}_i$ $(i = 1, 2, ..., k)$ used in the CFD calculations are determined from a series of structure calculations of a flexible plate subjected to a series of uniform pressures as follows.

2.2 Determination of $f(\tilde{\alpha})$

In order to determine the correction function $f(\tilde{\alpha})$, a series of numerical calculations of structure

mechanics and CFD calculations are conducted using commercially available codes of MSC Marc2010 and ANSYS Fluent 13.0, respectively. Firstly, a flexible plate subjected to a series of uniform pressures are conducted to determine a series of related reconfigurations of the plate. Large deformation, namely, the geometrical nonlinearity of the deformation is considered. The pressure applied to the flexible plate is given by below equation

$$p_i = \frac{1}{2} \rho V_i^2 C_D, \quad (0 < V_i \le V_{\max};\ i = 1, 2, \cdots, k) \tag{7}$$

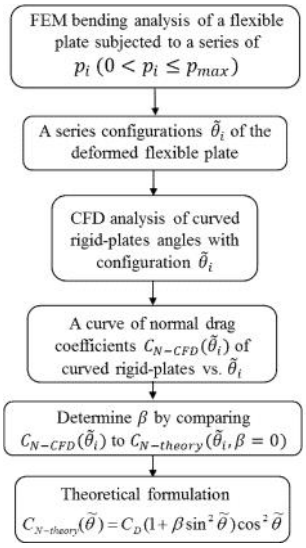

Fig. 2. Flowchart of the theoretical modeling.

Where $V_i\ (i = 1, 2, \cdots, k)$ denote a series of given wind velocities, $V_{\max}$ is the maximum velocity specified according to the design requirement of the flexible plate, and C_D is the drag coefficient of a rigid flat-plate normal to the flow as mentioned before. Then, applying $p_i\ (i = 1, 2, \cdots, k)$ of Eq. (7) to a given flexible plate and conducting the analysis of structure mechanics, we can obtain a series of self-similar geometries $\tilde{\theta}_i\ (i = 1, 2, \cdots, k)$ of curved plates. According to the experimental facts reported in many references as mentioned above, it is well known that the value of the real normal drag coefficient $C_{Ni-real}$ of a flexible flat-plate normal to the flow is always smaller than C_D because the deformation of the flexible plate reduces the drag force. Therefore, for a given V_i, the real averaged pressure p_{i-real} acting on a flexible plate is always lower than p_i calculated by Eq. (7) because $C_{Ni-real} < C_D$. In other words, the p_i gives the upper bound of p_{i-real} for a given V_i. Similarly, the chord angle $\tilde{\theta}_i$ of the deformed plate, obtained from the above structure analysis related to p_i, is also not equal to the real chord angle $\tilde{\theta}_{i-real}$ for a given V_i. The real chord angle $\tilde{\theta}_{i-real}$ is always smaller than $\tilde{\theta}_i$ and $0 < \tilde{\theta}_{i-real} < \tilde{\theta}_i$ because $0 < p_{i-real} < p_i$ for a given V_i. Hence, $\tilde{\theta}_i$ also gives the upper bound of $\tilde{\theta}_{i-real}$ for a given V_i.

Secondly, we use these curved plates with chord angles $\tilde{\theta}_i\ (i = 1, 2, \cdots, k)$ as a series of rigid curved-plates in the CFD calculations to solve the corresponding normal drag coefficients $C_{Ni-CFD}(\tilde{\theta}_i)\ (i = 1, 2, \cdots, k)$. That is, we obtain a curve of $C_{Ni-CFD}(\tilde{\theta}_i)\ (i = 1, 2, \cdots, k)$ related to a series of rigid curved-plates with chord angles $\tilde{\theta}_i\ (i = 1, 2, \cdots, k)$. On the other hand, according to Eq. (4) and Eq. (6) with $= 0$, we can obtain the theoretical formulation of normal drag coefficien $C_{N-theory}(\tilde{\theta})\big|_{=0}$. In consequence, we obtain two curves of $C_{N-CFD}(\tilde{\theta}_i)$ and $C_{N-theory}(\tilde{\theta})\big|_{=0}$. Plotting these two curves together and comparing them with each other reveal the deference between these two curves. Finally, select a proper value of through a process of trial and error to make the difference between these two curves as small as possible. That is, select a to make

$$C_{N-theory}(\tilde{\theta})\big| = C_D f(\tilde{\theta})\big| \cos^2\tilde{\theta} \approx C_{N-CFD}(\tilde{\theta}) \tag{8}$$

Then, Eq. (4) becomes a theoretical equation to predict the normal drag coefficient $C_{N-theory}(\tilde{\theta})$ for a known rigid curved-plate with chord angle $\tilde{\theta}_i$. The flow chart of the present theoretical modelling is described in Fig. 2.

2.3 Algorithm to Solve the Average Pressure Acting on a Flexible Plate Normal to the Flow

Assume that the geometry and material properties of a flexible plate are known, the velocity of uniform and steady wind inflow is V_0, and the plate normal to the flow is at a quasi-static state. Then, the real average pressure in the sense of FSI can be expressed by

$$p_{-real} = p_{\_theory}(\tilde{\theta}_{-bend}), \tag{9-1}$$

if the following equation is satisfied.

$$p_{\_theory}(\tilde{\theta}_{-bend}) = p_{\_bend}, \tag{9-2}$$

where, $p_{\_bend}$ denotes the pressure applied to the flexible plate in the structural analysis, $\tilde{\theta}_{-bend}$ is the corresponding chord angle of the deformed plate, and $p_{\_theory}(\tilde{\theta}_{-bend})$ is the theoretical average pressure obtained from Eq. (3). It is noted that the theoretical average pressure is approximately equal to the average pressure

obtained from CFD analysis of a rigid curved-plate with chord angle $\tilde{\theta}_{-bend}$ based on the preceding

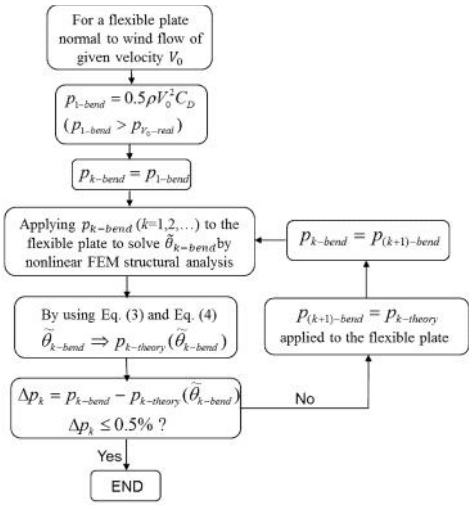

Fig. 3. Flowchart of the calculation sequence of the present approximate method.

theoretical modelling. In other words, Eq. (9-1) means that the real pressure equals the theoretical pressure obtained from Eq. 3 when the pressure applied to the flexible plate in the structure calculation equals the theoretical pressure acting on the rigid curved-plate with the chord angle $\tilde{\theta}_{-bend}$. Then, based on Eq. (9), an algorithm is developed to solve the real pressure p_{i-real}, chord angle $\tilde{\theta}_{i-real}$, and normal drag coefficient $C_{N-real}(\tilde{\theta}_{-real})$ for a flexible plate normal to the wind flow of V_0 using only iterative simulations of structure analysis as follows. V_0 is an arbitrary given wind velocity. The flowchart of calculation procedures of the approximate method is illustrated in Fig. 3.

At the first iteration, nonlinear bending calculation of the flexible plate subjected to a given pressure is conducted. The initial pressure is calculated by Eq. (6), that is,

$$p_{1\_bend} = \frac{1}{2} \rho V_0^2 \times C_D \tag{10}$$

Where the drag coefficient C_D of a rigid plate normal to the wind flow is obtained from CFD analysis for the rigid plate with the same geometry as the flexible plate. Then, a reconfiguration $\tilde{\theta}_{1-bend}$ of the flexible plate is obtained from the bending analysis. Inserting this $\tilde{\theta}_{1-bend}$ into Eq. (3) and Eq. (4) yields $p_{1\_theory}(\tilde{\theta}_{1-bend})$ and $C_{N1\_theory}(\tilde{\theta}_{1-bend})$, respectively. According to the preceding subsections, p_{1_bend} and $\tilde{\theta}_{1-bend}$ give the upper bounds of the real pressure p_{V_0-real} and real reconfiguration $\tilde{\theta}_{V_0-real}$, respectively. Therefore, p_{1_theory} obtained from Eq. (4) using $\tilde{\theta}_{1-bend}$ gives the lower bound of the real pressure. It is obvious that p_{1_bend} is not equal to p_{1_theory}. Thus, we move to the second iteration using p_{1_theory} as the bending load applied to the flexible plate as follows.

$$p_{2\_bend} = p_{1\_theory} \tag{11}$$

Similar to the calculation procedures at the first iteration, $\tilde{\theta}_{2-bend}$ is obtained from the bending calculation, and then $p_{2\_theory}(\tilde{\theta}_{2-bend})$ and $C_{N2\_theory}(\tilde{\theta}_{2-bend})$ can be obtained from Eq. (3) and Eq. (4). It is observed that

$$\begin{aligned} &\because \ \tilde{\theta}_{1-bend} > \tilde{\theta}_{2-bend} > 0 \\ &\therefore \ C_{N1-theory}(\tilde{\theta}_{1-bend}) < C_{N2-theory}(\tilde{\theta}_{2-bend}) < C_D \\ &\therefore \ p_{1\_bend} > p_{2\_theory}(\tilde{\theta}_{2-bend}) > p_{2\_bend} \end{aligned} \tag{12}$$

Assume that $p_{2\_theory}(\tilde{\theta}_{2-bend})$ is still not equal to p_{2_bend} and that the difference between the both values is still significant. Thus, we move to the third iteration using

$$p_{3\_bend} = p_{2\_theory} \tag{13}$$

as the pressure applied to the flexible plate in the bending calculation of the third iteration. Similar to preceding iterations, $\tilde{\theta}_{3-bend}$ is obtained from bending calculation, and then a set of $p_{3\_theory}(\tilde{\theta}_{3-bend})$, and $C_{N3\_theory}(\tilde{\theta}_{3-bend})$ are obtained using Eq. (3) and Eq. (4), respectively. It is observed that

$$\begin{aligned} &\because \ \tilde{\theta}_{1-bend} > \tilde{\theta}_{3-bend} > \tilde{\theta}_{2-bend} \\ &\therefore \ C_{N1-theory}(\tilde{\theta}_{1-bend}) < C_{N3-theory}(\tilde{\theta}_{3-bend}) < C_{N2-theory}(\tilde{\theta}_{2-bend}) \\ &\therefore \ p_{1\_bend} > p_{3\_bend} > p_{3\_theory}(\tilde{\theta}_{3-bend}) > p_{2\_bend} \end{aligned} \tag{14}$$

We must move to the next iteration if the difference between p_{3_bend} and $p_{3\_theory}(\tilde{\theta}_{3-bend})$ is still significant. Similar to the preceding iterations, iteratively repeat the computational procedures as described above until the difference between the theoretical pressure $p_{k\_theory}(\tilde{\theta}_{k-bend})$ obtained from Eq. (3) and the pressure p_{k_bend} applied to the flexible plate in the bending calculation at the *k*-th iteration is equal to or less than a given small value. In this study, the iterative calculation is completed when this difference satisfies the following criterion.

$$\Delta p = \frac{\left| p_{k\_theory} - p_{k\_bend} \right|}{\left| p_{k\_thoery} \right|} = \frac{\left| p_{k\_theory} - p_{k-1\_theory} \right|}{\left| p_{k\_thoery} \right|} \le 0.5\% \quad (15)$$

Therefore, based on Eq. (15) the real pressure acting on the given flexible plate normal to the wind flow of V_0 is defined by following equation.

$$p_{V_0-real} = p_{k\_theory} \quad (16)$$

3. NUMERICAL SIMULATION TESTS

In order to demonstrate the validity of the proposed approximate method, numerical simulation tests for several 3D flexible plates with different geometries and different material moduli were conducted using the approximate method. Furthermore, simulation for a 3D flexible plate studied by Gosselin *et al*. 2010 was also carried out for a comparison.

3.1 Simulation Tests for Five Flexible Plates

A 3D model of flexible plates normal to the wind flow is depicted in Fig. 4. The upper end of the model is clamped and the lower end is free. The length, width and thickness of the plate model are denoted by L, W and T, respectively. Five plates with different lengths or different material constants are used in the simulation tests. Table 1 and Table 2 give the geometries of five

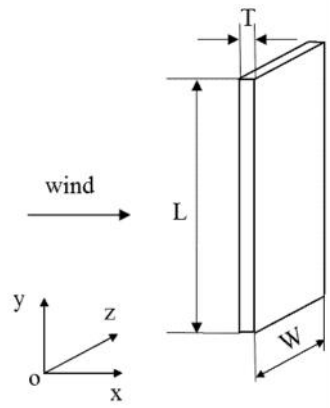

Fig. 4. A 3-D simulation model.

plates and the material constants of three kinds of materials. PP, PE and PET are the abbreviations of polypropylene, polyethylene and polyethylene terephthalate.

Following the computational procedures described in Section 2, the determination of the theoretical curve of $C_{N-theory}(\tilde{\ }) \approx C_{N-CFD}(\tilde{\ })$ is firstly carried out based on the theoretical modelling with the aid of a series of structural and CFD analyses. Then, iterative calculations of bending analysis are conducted to solve the real averaged pressure acting on the flexible plate and the deformation of the plate for a series of given wind velocities according to the algorithm of the approximate method. Both of structure and CFD analyses are ordinary calculations with definite boundary conditions and easily to be performed, which are relatively simple compared to complex conventional iterative fluid-structure coupling calculations.

Table 1 Geometries of five flexible thin plates

Plate	L (mm)	W (mm)	T (mm)
PP-100	100	100	1
PP-300	300	100	1
PP-500	500	100	1
PE-300	300	100	1
PET-300	300	100	1

Table 2 Material constants of three materials

Material	Young's Modulus (GPa)	Poisson's ratio	Density (10^3kg/m^3)
PE	0.392266	0.41	0.91
PP	1.569064	0.41	0.91
PET	3.010642	0.39	1.39

In the CFD analysis, the undisturbed inflow is assumed as uniform and the fluid is assumed to be incompressible. The computation domain of CFD analysis is 42L×24L ×11W with the origin of the coordinates located at the center of the plate, as shown in Fig. 5. The inlet, top, and bottom boundary walls are set at the distance of 12L from the center of the plate, respectively. The outlet is set at 30L downstream from the plate center. A uniform velocity flow is specified at the inlet, zero pressure is specified at outlet, slip condition is specified along the top and bottom boundary walls, and no-slip condition is specified on the plate surface. The large eddy simulation (LES) method is utilized in the CFD analysis. According to ANSYS Fluent 13.0 User's Guide (2010), in present CFD analysis, the Reynolds number *Re*, the turbulence intensity *I*, the turbulent kinetic energy *k*, and the turbulent length scale *l* are calculated as follows:

$$\mathrm{Re} = °VL / « \quad (17)$$

$$I = 0.16 \times (\mathrm{Re})^{-0.125} \quad (18)$$

$$k = 1.5 \times (VI)^2 \quad (19)$$

$$l = 0.07L \quad (20)$$

Where μ (= 1.8×10^{-5} Pa· s) is the viscosity coefficient of air at 20 degrees Celsius. The effect of the number of grids on the calculation accuracy is investigated firstly using the geometry of PP-500

plate with different numbers of grids from 1,133,500 to 5,269,000. The plate is assumed to be rigid and normal to the wind flow. The drag coefficient is calculated for each case of grid number. As the result, the number of grids around 2,500,000 is adopted for all the plates based on the considerations of acceptable computational accuracy and cost. Fig. 5(b) demonstrates a typical grid distribution around the rigid curved-plate of PP-300 and the total number of grids of the computational domain is 2,266,000.

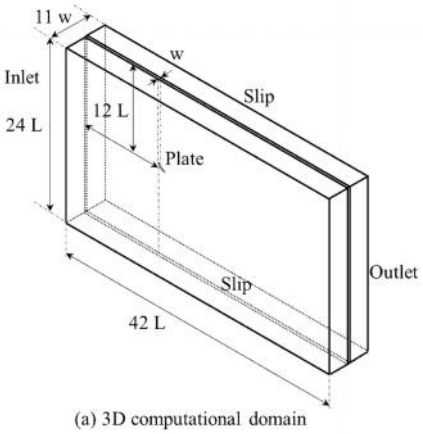

(a) 3D computational domain

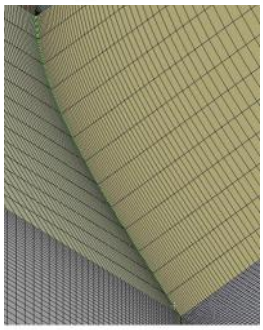

(b) Grid around the plate

Fig. 5. CFD computational domain (a) and grid around the plate (b).

3.2 A Comparative Simulation Test

A comparative simulation test of a 3D flexible plate used in a previous wind tunnel experiment by Gosselin *et al.* (2010), as shown in Fig. 6, is also conducted based on the present approximate method to confirm the validity of the approximate method. The length and width of the plate are 100 mm and 35 mm, respectively. The flexural rigidity of the plate is 10^{-6} Nm. The Young's modulus E = 3.1 GPa and Poisson's ratio ³ = 0.3 are used. In order to keep the same flexural rigidity as that used in the experiment of Gosselin *et al.* (2010), the thickness h of the plate is 0.0152 mm determined from the following equation.

$$\frac{Eh^3}{12(1-\neg^2)} = 10^{-6}\ (\text{Nm}) \tag{21}$$

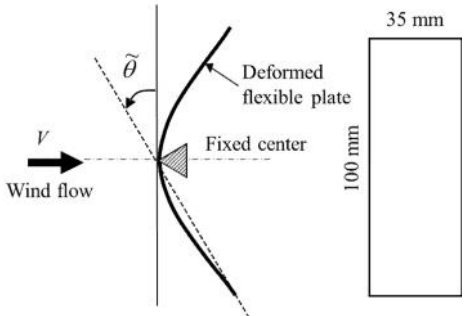

Fig. 6. Simulation model for the comparative test.

The computational domain for the comparative simulation test is a square section duct with 0.180 m in width and 4 m in length according to the experiment of Gosselin *et al.* (2010). The boundary conditions on the inlet, outlet, plate surface and boundary walls are the same as described in Fig. 5(a). The calculation procedures of the simulation test are the same as those described in subsection 3.1.

4. RESULTS AND DISCUSSION

Numerical results of simulation tests are presented in the following figures. Effects of the number of grids on the drag coefficient of a 3D vertical rigid plate of 500 mm in length, 100 mm in width, and 1 mm in thickness are described in Fig. 7. It is seen that the drag

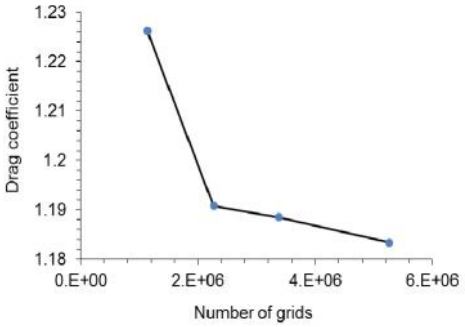

Fig. 7. Effect of the number of grids on the calculation results.

coefficient varies slowly and tends to converge a stable value when the number of grids is larger than 2,000,000. As the result, the grid number around 2,500,000 was adopted for the CFD analyses of all plates based on the considerations of acceptable computational accuracy and cost.

Following the analysis procedures as described in section 2, the theoretical curve $C_{N\_theory}(\tilde{\ })$ with = 0.5 is determined with the aid of structure and CFD analyses of five flexible plates listed in Table 1. The curve and the normal force coefficients obtained from the CFD analyses of five plates are presented in Fig. 8.

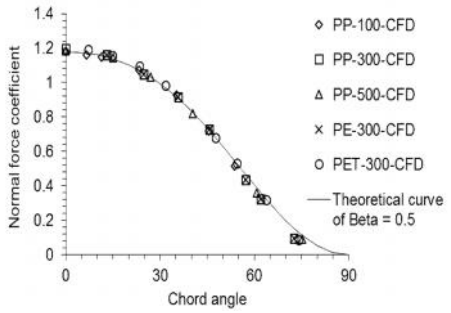

Fig. 8. Theoretical curve of normal force coefficient vs. chord angle of rigid curved-plates.

The normal force coefficients obtained from the CFD analyses of five plates are displayed by five kinds of marked points and the solid curve is the theoretical curve. It is obvious that the theoretical curve agrees well with the results obtained from the CFD analyses of five plates with different length or different modulus, although relatively large difference can be found for large chord angle beyond 60 degree. Therefore, it is reasonable that using the proposed theoretical modeling method to predict the relationship between the normal force coefficient and the chord angle of rigid curved-plate. We can calculate the normal force acting on a rigid curved-plate based on the theoretical curve if we know the chord angle of the curved-plate. In the case of very large chord angle which means large bending deformation of the plate, the theoretical curve overestimates the normal force. For a more accurate prediction of the normal force in the chord angle range of larger than 60 degree, a different parameter may be selected. That is, the theoretical curve may be defined in two ranges of chord angle: $0 \le \tilde{\ } < 60$ and $60 \le \tilde{\ } \le 90$, selcting different for different range. This issue is a further research subject which is ongoing now.

Results of the normal forces acting on the flexible plates and the deformations of the plates are presented versus to wind velocity in following figures. Effects of the plate length on the normal force acting on the three flexible plates at various wind velocities are depicted in Fig. 9. The CFD analysis results of normal force acting on the three PP plates with lengths of 100 mm. 300 mm, and 500 mm are compared with those obtained from the present approximate method. Here, the results of CFD analyses are obtained from the analysis of 3D rigid curved-plates which have the same geometries obtained from the approximate method. An enlarged draft for the data at low wind velocities is also presented below. Marked points denote the CFD results and solid, dashed and dotted curves denote the results of approximate method. It is seen that, when the wind velocity is lower than 5 m/s, the longest plate of PP-500 gives the largest normal force because of its largest area normal to the wind flow. However, as the wind velocity increases, the normal forces acting on the relatively short plates of PP-100 and PP-300 increase more rapidly and successively exceed the normal force acting on the longest plate of PP-500. The normal force acting on the shortest plate of PP-100 has the largest value at the wind velocities higher than 22 m/s and the longest plate

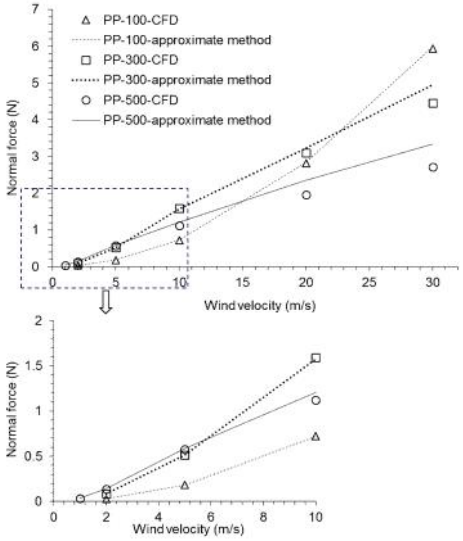

Fig. 9. Effects of the plate length on the normal force acting on the flexible plates at different wind velocities.

of PP-500 gives the smallest one. Furthermore, it is seen that both results obtained from the present approximate method and the CFD analysis are in good agreement, especially in the case of PP-100 plate. In the cases of PP-300 and PP-500 plates, the difference between both results increases with the increase of wind velocity. These features reflect the effects of the bending deformations of flexible plates on the normal force acting on the plates. Longer plate is easily bended by the wind flow than shorter one at the same wind velocity. Larger bending chord angle leads to lower normal force acting on the bended plate. For a more accurate prediction of the normal force acting on the flexible plate with a large chord angle, a different parameter may be selected, as mentioned above. In addition, the average pressure acting on the plates can be calculated by the normal force divided by the plate area, referring to Eq. (3b).

Effects of material modulus on the normal force acting on the three flexible plates with the same geometry but different moduli are described in Fig. 10. The normal forces acting on a rigid plate having the same geometry are also depicted in the figure for a comparison. Similar to Fig. 9, the results obtained from the present approximate method agree well with those obtained from the CFD analyses. The normal force acting on the PET-300 which has the highest modulus increases quickly. In contrast, the normal force acting on the PE-300 which has the lowest modulus increases slowly. Plate with high modulus is hard to be bended by wind flow compared to the plate with low modulus. Large bending deformation reduces the normal force acting on the bended plate. These results are

in consistence with the nature phenomena frequently observed from the bended trees under high wind.

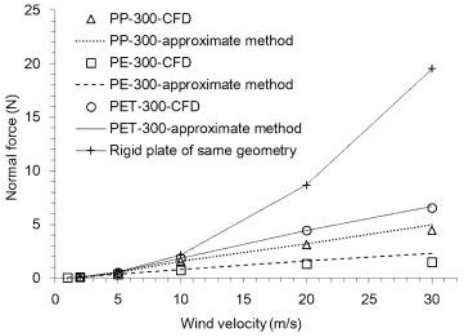

Fig. 10. Effect of material modulus on the normal force acting on the flexible plates at various wind velocities.

The chord angles of five bended flexible plates at various wind velocities, obtained from the present approxvimate method, are described in Fig. 11. It is clear that the flexible plate with low modulus or large length has large chord angle which means large bending deformation.

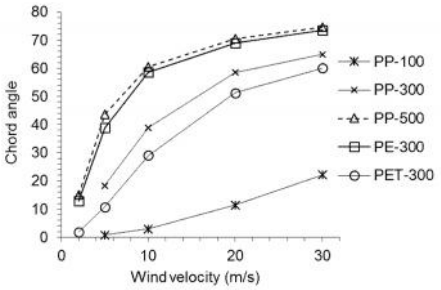

Fig. 11. Chord angles of five flexible plates at various wind velocities.

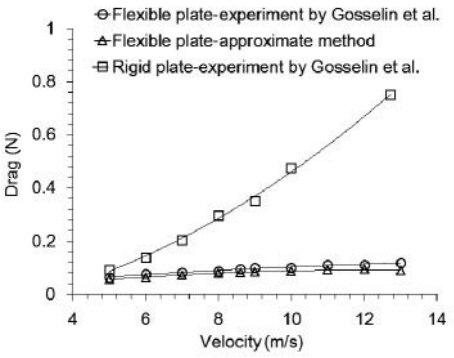

Fig. 12. Comparison of drag force obtained from the previous experiment and the present approximate method.

Finally, the results of drag force obtained form the comparative simulation are compared with the previous experimental results (Gosselin *et al*. (2010)) in Fig. 12. The drag force of a rigid plate obtained from the previous experiment is also depicted for a contrast. The drag values obtained from the present approximate method are well consistent with the previous experiment results. These comparative simulation results further confirm the validity and accuracy of the present approximate method.

5. CONCLUSION

Based on the theoretical modelling, the construction of the approximate method, and the numerical simulation tests, this study leads to following conclusions.

- An explicit theoretical formulation for the prediction of the curve of the normal drag coefficient of a rigid curved-plate versus to its chord angle is derived through a theoretical moldelling with the aid of a series of ordinary nonlinear structure mechanics and CFD analyses.. The formulation is simple and gives good accuracy of pridiction. Further study is needed to improve the prediction accuracy by selecting different correction parameters for different chord angle ranges.
- An approximate method to evaluate the normal force acting on a flexible flat-plate normal to the wind flow and the deformation of the plate is developed using the present theoretical formulation and the iteration of only structure analyses instead of complex fluid-structure coupling analysis.
- Results of the numerical simulation tests for the plates with different geometries and material moduli demonstrate the validity and accuracy of the approximate method. Moreover, the comparative simulation test of a 3D flexible plate used in a previous wind tunnel experiment further confirm the accuracy of the present approximate method. Therefore, it is considered that the present approximate method is relatively simple compared to conventional complex fluid-structure coupling analysis and is useful for the evaluation of the normal force acting on the flexible plate normal to the wind flow and the deformation of the plate in the practice applications.

REFERENCES

Alben, S., M. Shelley and J. Zhang (2002). Drag reduction through self-similar bending of a flexible body. *Nature* 420(6915), 479-481.

Alben, S., M. Shelley and J. Zhang (2004). How flexibility induces streamlining in a two-dimensional flow. *Physics of Fluids* 16(5), 1694-1713.

Breuer, M., N. Jovicic and K. Mazaev (2003). Comparison of DES, RANS and LES for the separated flow around a flat plate at high incidence. *International Journal for Numerical* 41, 357-388.

Campbell, R. L. and E. G. Paterson (2011). Fluid–

structure interaction analysis of flexible turbomachinery. *Journal of Fluids and Structures* 27, 1376-1391.

Chein, R. and J N. Chung (1988). Discrete-vortex simulation of flow over inclined and normal plates. *Computers & fluids* 16(4), 405-427.

Degroote, J. (2013). Partitioned Simulation of Fluid-Structure Interaction. *Archives of Computational Methods in Engineering* 20, 185-238.

Fage, A. and F. C. Johansen (1927). On the flow of air behind an inclined flat plate of infinite span. *Proceedings of the Royal Society of London, Series A* 116, 170-197.

Feng, Z. G. and E. E. Michaelides (2004). The immersed boundary-lattice Boltzmann method for solving fluid–particles interaction problems. *Journal of Computational Physics* 195(2), 602-628.

Gosselin, F., E. de LANGRE and B. A. Machado-Almeida (2010). Drag reduction of flexible plates by reconfiguration. *Journal of Fluid Mechanics* 650, 319-341.

Hoogedoorn, E., G. B. Jacobs and A. Beyene (2010). Aero-elastic behavior of a flexible blade for wind turbine application: A 2D computational study. *Energy* 35(2), 778-785.

Hou, G., J. Wang and A. Layton (2012). Numerical Methods for Fluid-Structure Interaction - A Review. *Communications in Computational Physics* 12(2), 337-377.

Kim, Y. and C. S. Peskin (2007). Penalty immersed boundary method for an elastic boundary with mass. *Physics of Fluids* 19(5), 053103.

Kinsely, C. W. (1990). Strouhal numbers of rectangular cylinders at incidence: A review and new data. *Journal of Fluids and Structures* 4, 371-393.

Kiya, M. and M. Arie (1977). An inviscid numerical simulation of vortex shedding from an inclined flat plate in shear flow. *Journal of Fluid Mechanics* 82(02), 241-253.

Lee, J. S. and S. H. Lee (2012). Fluid–structure interaction analysis on a flexible plate normal to a free stream at low Reynolds numbers. *Journal of Fluids and Structures* 29, 18-34.

Letchford, C. W. (2001). Wind loads on rectangular signboards and hoardings. J*ournal of Wind Engineering and Industrial Aerodynamics* 89, 135-151.

Liu, Z. and Y. L. Young (2009). Utilization of bend–twist coupling for performance enhancement of composite marine propellers. *Journal of Fluids and Structures* 25(6), 1102-1116.

Maheri, A., S. Noroozi and J. Vinney (2007). Combined analytical/FEA-based coupled aero structure simulation of a wind turbine with bend–twist adaptive blades. *Renewable energy* 32(6), 916-930.

Okajima, A. (1990). Numerical simulation of flow around rectangular cylinders. *Journal of Wind Engineering and Industrial Aerodynamics* 33(1), 171-180.

Peskin, C. S. (2002). The immersed boundary method. *Acta numerica* 11, 479-517.

Schouveiler, L. and A. Boudaoud (2006). The rolling up of sheets in a steady flow. *Journal of Fluid Mechanics* 563, 71-80.

Shimada, K. and T. Ishihara (2002). Application of mpdified $k-£$ model to yhe prediction of aerodynamic characteristics of recyangular cross-section cylinders. *Journal of Fluids and Structures* 16(4), 465-485.

Vogel, S. (1989). Drag and Reconfiguration of Broad Leaves in High Winds. *Journal of Experimental Botany* 40, 941-948.

Vogel, S. (2009). Leaves in the lowest and highest winds: temperature, force and shape. *New Phytologist* 183(1), 13-26

White, F. (1998). *Fluid Mechanics (Fouth Edition).* University of Rhode, Kingstone 458-460.